satisfactory image (Fig. 8). An example of a dislocation in silicon is shown in Fig. 9.

This automatic switching cannot be used for extended defects, since it is not possible to establish a refined network as shown in Fig. 6: the defect intersects the transmitted beam in all planes of incidence and one must rebuild a different refined network for each incidence plane. The best method is to use the Φ method for the nodes between the direct image and $\mathbf{s}_h$ and the Ψ method near $\mathbf{s}_0$. The only difficulty is that one must switch between the integration formulae (13) and (14). This means, as indicated in (3), that one must change the phase of the wave in the middle of the integration process. This may be rather delicate since the phase between two adjacent nodes in the integration network may vary more rapidly than the modulus of the amplitudes. This means that one must be very careful about the length of the steps of integration. No general values can be given since it depends on the kind of material and deformation and only a trial-and-error method maybe used. We have used this method to simulate the images of quartz piezoelectric resonators and we found after many tests that the step sizes could be used for all the simulations independently from the diffraction parameters (Carvalho, 1990).

Concluding remarks

In the present paper, we describe a new numerical algorithm to integrate Takagi–Taupin equations when the incident wave is not a plane wave. We have been able to estimate the error term and minimize it by using two different forms of the equations in the numerical computation. This new method presents two advantages.

(i) It is more accurate than the usual Tournarie method. As we will show in our next paper (Carvalho & Epelboin, 1993), it allows use of the theorem of reciprocity to simulate traverse and synchrotron topographs, which has not been possible before. There are many advantages to this, which will be explained in this paper.

(ii) It is faster since it needs less operations. The computing time is halved. It is now possible to compute section topographs on a good modern microcomputer. An image may be calculated in a few minutes and requires only a modest-size memory.

This method enables the simulation of section and traverse topographs to cover extended defects since now the simulation of the direct image is much more satisfactory.

CAMC acknowledges a doctorate scholarship from CNPq, Brazil.

References

ARISTOV, V. V., KOHN, V., POLOVINKINA, V. I. & SNIGIREV, A. A. (1982). *Phys. Status Solidi A*, **72**, 483-491.
AUTHIER, A., MALGRANGE, C. & TOURNARIE, M. (1968). *Acta Cryst.* A**24**, 126-136.
BALIBAR, F. (1969). *Acta Cryst.* A**25**, 650-658.
CARVALHO, C. A. M. (1990). Thesis, Univ. P. M. Curie, Paris, France.
CARVALHO, C. A. M. & EPELBOIN, Y. (1990). *Acta Cryst.* A**46**, 449-459.
CARVALHO, C. A. M. & EPELBOIN, Y. (1993). *Acta Cryst.* A**49**, 467-473.
EPELBOIN, Y. (1981). *Acta Cryst.* A**37**, 132-133.
EPELBOIN, Y. (1985). *Mater. Sci. Eng.* **73**, 1-43.
EPELBOIN, Y. & PATEL, J. R. (1982). *J. Appl. Phys.* **53**, 271-275.
EPELBOIN, Y. & SOYER, A. (1985). *Acta Cryst.* A**41**, 67-72.
NOURTIER, C. & TAUPIN, D. (1981). *J. Appl. Cryst.* **14**, 432-436.
PETRASHEN, P. V. (1976). *Sov. Phys. Solid State*, **18**, 2175-2176.
PETRASHEN, P. V., CHUKHOVSKII, F. N. & SHULPINA, I. L. (1980). *Acta Cryst.* A**36**, 287-295.
TAKAGI, S. (1969). *J. Phys. Soc. Jpn*, **26**, 1239-1253.
TAUPIN, D. (1967). *Acta Cryst.* **23**, 25-35.

Acta Cryst. (1993). A**49**, 467-473

Simulation of X-ray Traverse Topographs and Synchrotron Laue Topographs: Application of the Reciprocity Theorem

BY C. A. M. CARVALHO AND Y. EPELBOIN

Laboratoire de Minéralogie-Cristallographie, Universités P. M. Curie et Paris VII, *UA* 009, *CNRS, Case* 115, 75252 *Paris CEDEX* 05, *France*

(*Received* 21 *July* 1992; *accepted* 8 *October* 1992)

Abstract

A new demonstration of the reciprocity theorem of optics in the case of the X-ray dynamical theory is given. It is applied to the simulation of traverse and white-beam synchrotron topographs. It is shown that the accuracy of a new numerical algorithm [Carvalho & Epelboin (1993). *Acta Cryst.* A**49**, 460-467] allows

0108-7673/93/030467-07$06.00

the use of the reciprocity theorem. Its main advantage is to decrease the time of computation by at least an order of magnitude and to permit a strategy to be built for the quantitative study of defects, starting with simulations of poor resolution and increasing resolution only in worthwhile areas. This was not possible with the previous method.

I. Introduction

In our preceding paper (Carvalho & Epelboin, 1993), we explained how the Takagi–Taupin equations (Takagi, 1969; Taupin, 1967) may be numerically computed using a new algorithm that is more accurate than the previous ones (Authier, Malgrange & Tournarie, 1968; Petrashen, 1976). In this paper, we will discuss its use for the simulation of traverse and white-beam synchroton topographs.

Carvalho & Epelboin (1990) explained that, in most experiments, the contrast may be explained as the addition of the contribution of incoherent point sources distributed along the entrance surface of a crystal. This is due to the large source-to-crystal distance. It might not be true for low-emittance rings but this will be visible only in small regions of the image in which the contrast varies rapidly and it is doubtful that this difference will be visible in the experiments. This means that, for most white-beam Laue topographs, it is possible, to a very good approximation, to interpret the contrast formation and to simulate the images in the same manner as for traverse topographs made in the laboratory.

Traverse topographs may be computed either by addition of the contribution of point sources distributed along the entrance surface of the crystal or by application of the reciprocity theorem of optics. The latter method presents many advantages since it is possible to choose the sampling of the pixels in the computed image independently of the distribution of point sources, which is not true for the former method. This will be explained in detail in § III. Petrashen, Chukovskii & Shulpina (1980) attempted to compute a line through a traverse topograph using the reciprocity theorem but the intensity in the darkest parts of the image was strongly underestimated. Epelboin & Soyer (1985) showed that this was due to the limited precision of the numerical algorithms and were able to simulate whole images using the Tournarie algorithm (Authier, Malgrange & Tournarie, 1968) and summing the contribution of point sources. Nobody, up to now, has been able to use the reciprocity theorem for image simulation.

In this paper, we will explain how the new algorithm (Carvalho & Epelboin, 1993) allows the use of the reciprocity theorem. In § II we will present a new demonstration of this theorem then we will explain the principles of the simulation and present some computed images.

II. The reciprocity theorem

The first demonstration of the reciprocity theorem was given by Kato (1968) in the case of X-ray diffraction. It was explained in greater detail by Petrashen *et al.* (1980). We present here a new demonstration.

Let us consider two geometries (Fig. 1) for diffraction. In Fig. 1(*a*), a light source is located at point Q along the entrance surface of the crystal and we compute the intensity at point P on the exit surface. This will be called direct geometry. The incident beam propagates inside the crystal along $\mathbf{s}_0$ and $\mathbf{s}_h$ and the observation point is P. In Fig. 1(*b*), the situation is reversed: the observation point is Q, the light source is located at P and the incident beam propagates along $\tilde{\mathbf{s}}_0$, the reflected beam along $\tilde{\mathbf{s}}_h$. Both directions are reversed compared to Fig. 1(*a*) since $\tilde{\mathbf{s}}_0$ is parallel with $\mathbf{s}_h$ and $\tilde{\mathbf{s}}_h$ is parallel with $\mathbf{s}_0$. The reciprocity theorem says that a light source located at point Q (Fig. 1*a*) creates at point P a diffracted amplitude that is the same as if the light source were located at point P and the observation point at point Q (Fig. 1*b*). The reciprocity theorem does not say that the physical distribution of the amplitude of the light is equivalent in between these points, especially inside the crystal. It is simply concerned with an interchange of observation and source positions. This theorem is well known in optics but, to our knowledge, the only demonstration for diffraction (Landau & Lifchitz, 1960) concerns the total field, *i.e.* the sum of the refracted and reflected fields $\Phi_0+\Phi_h$ inside the crystal. Kato (1968) applies the theorem to the reflected field Φ_h only, considering that both the source and the observation points are far enough apart that the beams are separated.

The Takagi–Taupin equations are

$$\begin{aligned}\partial\Psi_0/\partial s_0 &= i2\pi K\beta_0\Psi_0 \\ &\quad - i\pi KC\chi_{\bar{h}}\exp(-i2\pi\mathbf{h}\cdot\mathbf{u})\Psi_h \\ \partial\Psi_h/\partial s_h &= i2\pi K\beta_h\Psi_h \\ &\quad - i\pi KC\chi_h\exp(i2\pi\mathbf{h}\cdot\mathbf{u})\Psi_0,\end{aligned} \tag{1}$$

where Ψ_h and Ψ_0 are the amplitudes of the diffracted

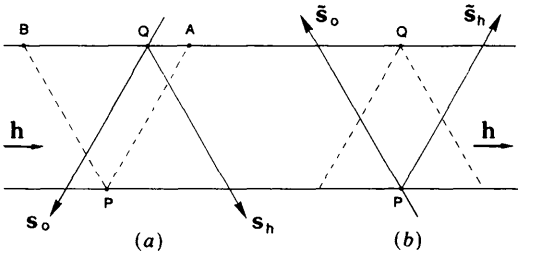

Fig. 1. (*a*) Direct geometry: a light source is located at Q, the intensity is computed at P. $\mathbf{s}_0$ and $\mathbf{s}_h$ are the transmitted and reflected directions, respectively. (*b*) Reciprocal geometry: the light source is located at P and the observation point at Q. The transmitted and reflected directions are reversed.

and transmitted waves, χ_h and $\chi_{\bar{h}}$ the Fourier components of the dielectric susceptibility, $\mathbf{h}$ the reciprocal-lattice vector for the studied reflection and $\mathbf{u}$ the deformation inside the crystal. $K=1/\lambda$ is the wave number of the beam incident on the crystal, $C=1$ or $\cos 2\theta$ is the usual polarization factor. In these equations, it is possible to choose the wave vectors so that β_0 and β_h match at their extremities:

$$\beta_0=[\mathbf{k}^2-K^2(1+\chi_0)]/2K^2$$

and

$$\beta_h=[(\mathbf{k}+\mathbf{h})^2-K^2(1+\chi_0)]/2K^2.$$

Usually, we choose $\beta_{h,0}=0$, which means that the wave vectors corresponding to the refracted and reflected directions inside the crystal have the same length, $|\mathbf{k}|=|\mathbf{k}+\mathbf{h}|=K(1+\chi_0)$.

We define Φ_h as $\Psi_h(P)=\Phi_h\exp(i2\pi\mathbf{h}\cdot\mathbf{u})$ and (1) become:

$$\partial\psi_0/\partial s_0=-i\pi KC\chi_{\bar{h}}\Phi_h,$$
$$\partial\Phi_h/\partial s_h=-i\pi KC\chi_h\Psi_0-i2\pi(\partial\mathbf{h}\cdot\mathbf{u}/\partial s_h)\Phi_h, \quad (2)$$

which may be written, with Ψ_0 eliminated, as the well known equation (Takagi, 1969)

$$\partial^2\Phi_h/\partial s_0\partial s_h+i2\pi(\partial/\partial s_h)(\mathbf{h}\cdot\mathbf{u})\partial\Phi_h/\partial s_0$$
$$+[\pi^2K^2C^2\chi_h\chi_{\bar{h}}+i2\pi(\partial^2/\partial s_0\partial s_h)\mathbf{h}\cdot\mathbf{u}]\Phi_h=0. \quad (3)$$

The boundary conditions are (Takagi, 1969):

$\Phi_h(\xi)=0$ along the entrance surface (Fig. 2);

$$\partial\Phi_h(\xi)/\partial s_h=-i\pi KC\chi_h(\gamma_0/\gamma_h)\Psi_e(\xi)$$
$$\times\exp[-i2\pi(\mathbf{K}\cdot\mathbf{r}_s-\mathbf{k}\cdot\mathbf{r}_s)]. \quad (4)$$

$\gamma_0=\cos\psi_0$, $\gamma_h=\cos\psi_h$ (Fig. 2), $\mathbf{r}_s$ is the position of a point along the entrance surface which may also be designated by its coordinate ξ along the surface, $\mathbf{k}$ is the wave vector inside the crystal and $\mathbf{K}$ is the wave vector of the incident wave. Ψ_e is the amplitude of the incident wave.

It is possible to solve (1) using a Riemann function (Authier & Simon, 1968). Takagi (1969) writes this Riemann function v as the solution of the integral equation

$$\Phi(P)=-(i\pi kC\chi_h/\sin 2\theta)\int_{BA}\gamma_0(\xi)v(P,\xi)\Psi_e(\xi)$$
$$\times\exp[-i2\pi(\mathbf{K}\cdot\mathbf{r}_s-\mathbf{k}\cdot\mathbf{r}_s)]\,d\xi, \quad (5)$$

where B, A and P are points as shown in Fig. 1(a). This Riemann function is the solution of the partial-derivative equation

$$\partial^2v(P,\mathbf{r})/\partial s_0\partial s_h-i2\pi(\partial\mathbf{h}\cdot\mathbf{u}/\partial s_h)[\partial v(P,\mathbf{r})/\partial s_0]$$
$$+\pi^2K^2C^2\chi_h\chi_{\bar{h}}v(P,\mathbf{r})=0. \quad (6)$$

$\mathbf{r}$ is the position of a point inside the crystal. The boundary conditions may be written as

$$v=\begin{cases}1 & \text{along } PA\\ \exp(-i2\pi\{\mathbf{h}\cdot[\mathbf{u}(\mathbf{r})-\mathbf{u}(P)]\}) & \text{along } PB.\end{cases} \quad (7)$$

Let us now consider the direct geometry (Fig. 1a). A point source is located at point Q, which means

$$\Psi_e(\xi)\exp[-i2\pi(\mathbf{K}\cdot\mathbf{r}_s-\mathbf{k}\cdot\mathbf{r}_s)]=\delta(\mathbf{r}_s-\mathbf{r}_{sQ}),$$

where $\mathbf{r}_{sQ}$ means the coordinate of point Q. Equation (5) becomes

$$\Phi(P)=-i\pi(KC\chi_h/\sin 2\theta)v(P,Q)$$
$$\equiv Fv(P,Q), \quad (8)$$

thus,

$$\Psi_h(P)=Fv(P,Q)\exp[i2\pi\mathbf{h}\cdot\mathbf{u}(P)]. \quad (9)$$

From (7), the boundary conditions are

$$\Phi_Q(P)=\begin{cases}F & \text{along } PA\\ F\exp(-i2\pi\{\mathbf{h}\cdot[\mathbf{u}(P)-\mathbf{u}(Q)]\}) & \\ & \text{along } PB,\end{cases} \quad (10)$$

where $\Phi_Q(P)$ means the amplitude of the diffracted wave at point P coming from the point source Q.

From the definition of Ψ_h, we may write

$$\Psi_Q(P)=\begin{cases}F\exp[i2\pi\mathbf{h}\cdot\mathbf{u}(Q)] & \\ \quad\times\exp(i2\pi\{\mathbf{h}\cdot[\mathbf{u}(P)-\mathbf{u}(Q)]\}) & \\ & \text{along } PA\\ F\exp[i2\pi\mathbf{h}\cdot\mathbf{u}(Q)] & \text{along } PB\end{cases} \quad (11)$$

and (3) becomes

$$\partial^2\Psi_h/\partial s_0\partial s_h-i2\pi(\partial\mathbf{h}\cdot\mathbf{u}/\partial s_0)(\partial\Psi_h/\partial s_h)$$
$$+\pi^2K^2C^2\chi_h\chi_{\bar{h}}\Psi_h=0. \quad (12)$$

Note that this equation resembles equation (6) for the Riemann function except that the axes $\mathbf{s}_0$ and $\mathbf{s}_h$ are reversed.

Let us now consider the reciprocal geometry (Fig. 1b). We call $\tilde{\Psi}_h$ the amplitude of the diffracted wave for this geometry. Equation (12) is still valid except that now the positions of the axes $\mathbf{s}_0$ and $\mathbf{s}_h$ are

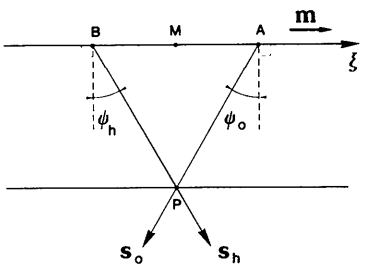

Fig. 2. Geometry for the diffraction equations. ζ lies along the entrance surface, ψ_0 and ψ_h are the angles between the normal to the entrance surface and $\mathbf{s}_0$ and $\mathbf{s}_h$, respectively.

reversed (Fig. 1*b*),

$$\partial^2\tilde{\Psi}_h/\partial\tilde{s}_0\partial\tilde{s}_h - i2\pi(\partial\mathbf{h}\cdot\mathbf{u}/\partial\tilde{s}_0)(\partial\tilde{\Psi}_h/\partial\tilde{s}_h) + \pi^2K^2C^2\chi_h\chi_{\bar{h}}\tilde{\Psi}_h = 0 \qquad (13)$$

with the transformations between the axes

$$\partial/\partial\tilde{s}_0 = -\partial/\partial s_h \qquad \partial/\partial\tilde{s}_h = -\partial/\partial s_0.$$

Equations (13) and (6) look exactly the same when written with coordinates s_0, s_h transformed in this way. P is now the position of the source, Q the position of the observation point and the directions of the transmitted and reflected beams are exchanged.

The boundary conditions are

$$\tilde{\Psi}_P(Q) = \begin{cases} F\exp[i2\pi\mathbf{h}\cdot\mathbf{u}(P)] & \text{along } PA \\ F\exp[i2\pi\mathbf{h}\cdot\mathbf{u}(P)] \\ \quad\times\exp(i2\pi\{\mathbf{h}\cdot[\mathbf{u}(Q)-\mathbf{u}(P)]\}) \\ \qquad\qquad\qquad\text{along } PB, \end{cases} \qquad (14)$$

which is exactly (7) except for a phase constant $F\exp[i2\pi\mathbf{h}\cdot\mathbf{u}(P)]$. We may now conclude that

$$\tilde{\Psi}_P(Q) = F\exp[i2\pi\mathbf{h}\cdot\mathbf{u}(P)]v(P,Q). \qquad (15)$$

By comparison of (15) and (9), it is clear that $\Psi_Q(P) = \tilde{\Psi}_P(Q)$, which is exactly what the theorem of reciprocity says.

III. Application to the simulation of traverse topographs

The simplest method to compute a traverse topograph or a synchrotron white-beam topograph is to add the contributions of individual point sources distributed along the entrance surface of the crystal (Epelboin & Soyer, 1985). This is called the direct method. Individual section topographs are calculated and the intensities are summed at each point P on the exit surface (Fig. 3). The distribution of sources along the entrance surface must be dense enough that the amplitude between two adjacent point sources varies slowly (Epelboin, 1977). For a perfect crystal, this means that this distance must be an order of magnitude smaller than the distance between two extinction fringes along the exit surface, *i.e.* less than 1 μm. Thus, one has to add the contributions along BA of numerous sources to be able to compute the intensity at point P. Practically, this means that individual section topographs, corresponding to all the point sources from A to B, are computed then summed to calculate the distribution of intensity along the exit surface from C to D (Fig. 3). The distance between two adjacent points along the exit surface corresponds to the distance between two adjacent sources along the entrance surface. This gives a resolution for the simulation that is far too high compared with experimental resolution; a tenth of the computed points would be enough for the final simulation.

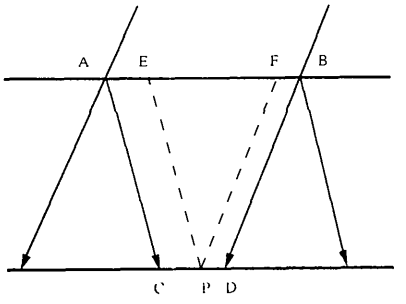

Fig. 3. The direct method. The total intensity at point P is the sum of all the contributions from the point sources distributed between E and F along the entrance surface. To compute a profile between C and D, one must add the contributions of the section topographs between A and B.

The computation time is enormous. Let us give some figures. Assume that the width of an image is 500 μm and that the distance between two point sources is 0.5 μm, which is an optimistic figure. For a crystal 800 μm thick and a Bragg angle of the order of 10°, the base of the Borrmann fan is about 250 μm, which means that AB is about 750 μm. Thus, 1500 section topographs must be added to compute each line in the image!

The reciprocity theorem allows the resolution in the image, *i.e.* the number of points in the computed line, to be decoupled from the density in the distribution of sources along the entrance surface. To compute the intensity at point P on the exit surface, the Riemann function is computed for this point by integration of (6) or, since it is the same, by computation of the diffracted amplitude along EF coming from a point source located at P in the reciprocal geometry (Fig. 3). Then, the intensity is summed from all the points along EF in this reciprocal geometry to find the total contribution at point P in the direct geometry. This is called the reciprocal method. The intensity at point P is known from a single integration of (13) and there is no longer any relation between the density of pixels, *i.e.* the number of points P in a line of the image and the density of sources along the entrance surface. This dramatically decreases the number of computations. With the same values as before, this means that, for a resolution of 2 μm in the image, it is sufficient to compute 250 section topographs. The computation time is decreased by a factor 6. In fact, the figures are better since it is only necessary to use such a resolution in areas of the image where the contrast varies rapidly. The width of the image of a dislocation, for instance, in a traverse or synchrotron topograph is never more than a few tens of micrometres. Thus, the best method is to compute a first simulation with a poor resolution then, in the areas where the contrast varies rapidly, to compute a second one with a better resolution. Thus, one may expect more than one order of magnitude less computation time.

Up to now, the accuracy of the numerical algorithms has not allowed the use of the reciprocity theorem. In a section topograph, the intensity in the direct image of the defect was underestimated and this led to wrong intensities in the image corresponding to a traverse topograph. This error was less visible when using the direct method (Epelboin & Soyer, 1985). In our preceding paper (Carvalho & Epelboin, 1993), we described a new algorithm that is more accurate than previous ones. We only summarize the conclusions here and show how the algorithm may be used in conjunction with the reciprocity theorem to compute traverse and synchrotron topographs.

Two different methods have been described: the 'Ψ method' and the 'Φ method'. With a standard network (*i.e.* a network similar for all incident planes without refining the network in the area where the direct image is created) for the integration of the Takagi–Taupin equations, both methods are valid if the minimum step is made much smaller than that usually satisfactory for the simulation of section topographs, *i.e.* a decrease from 0.2 to 0.025 μm along the exit surface of the crystal. We have shown that a better method is to use both methods together: in the planes of incidence where a direct image exists, the Ψ method is used for the nodes between the direct image and the diffracted beam and the Φ method is used for the other nodes. Switching between the two methods is done automatically using the criterion of validity of the geometrical optics (Balibar, 1969). In the other incidence planes, only the Ψ method is used.

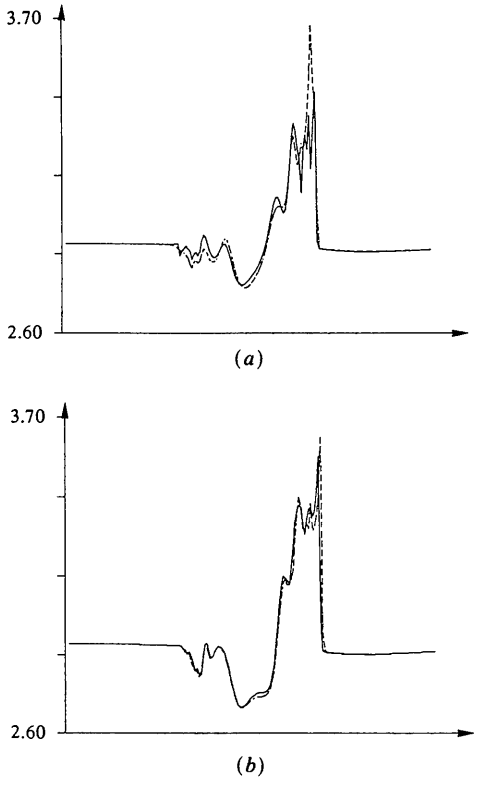

Fig. 4. Profile of intensity along a line in a traverse topograph. Silicon crystal 400 μm thick, Mo $K\alpha$ 220. The characteristics of the dislocation are the same as those studied by Epelboin & Soyer (1985). The thickness of the crystal was decreased for the computation. Solid line: reciprocal method; dashed line: direct method. (*a*) Standard network: minimum step along the exit surface 0.2 μm. (*b*) Standard network: minimum step 0.025 μm.

Fig. 4 presents the profile of intensity in a single line of a traverse topograph. A dislocation lies 100 μm under the surface of a silicon crystal 400 μm thick. This is the same crystal as that studied by Epelboin & Soyer (1985). Fig. 4(*a*) has been computed using a standard network and a minimum step length, along the exit surface, of 0.2 μm. This value is a reference since it is often satisfactory in most parts of the computation, except in the area where the direct image is created. The dashed line shows the profile computed using the direct method, *i.e.* by summation of the contributions of a distribution of point sources along the entrance surface. This is the method used previously by Epelboin & Soyer (1985). The solid line presents the result of the computation using the reciprocal method. It is obvious that the intensity in the direct image of the dislocation is strongly underestimated. Computation of the profiles with a step eight times smaller gave the same result for the two methods. This required a much longer computing time but, when using the reciprocal method, very few points in the image must be computed with this finer mesh. For Fig. 4(*b*), the direct method needed 60 times the time needed to compute the profile in Fig. 4(*a*). The reciprocal method, by combination of the two networks from Figs. 4(*a*) and (*b*), the one with the larger step in the areas where the intensity is low, the one with the smaller step in the area where the intensity is high, requires 3 min, which is about ten times less than the time needed when using the direct method for Fig. 4(*a*). This definitively shows the advantage of the reciprocal method. It should be noted that the convergence between the direct and the reciprocal methods was not previously possible by use of the Tournarie algorithm (Epelboin & Soyer, 1985).

IV. Simulation of traverse and synchrotron topographs

Fig. 5 shows the simulation of a Laue white-beam topograph. The original image shown in Fig. 5(*a*) was recorded at DCI LURE. It is a dislocation in a silicon crystal 800 μm thick, which was previously used as a test by Epelboin & Soyer (1985). Fig. 5(*b*) is the simulation, using the reciprocal method, with a representation distance between two adjacent pixels of 2 μm. The integration of the Takagi–Taupin equations was made with the standard network. The image was computed in two parts: first one pixel in three was calculated along a line and one line in two

along a column, then the critical part, *i.e.* around the direct image of the dislocation, which appears as a black vertical contrast, was computed for all the pixels. The two images were superimposed and are slightly visible because the background had to be renormalized between the two computations. The computation was performed with the standard network of integration and the quality of the image is satisfactory, although we know, from the previous study, that the intensity is underestimated in some parts of the direct image. This is not really visible since it corresponds to areas in a film where the maximum density of greys is reached.

(*a*)

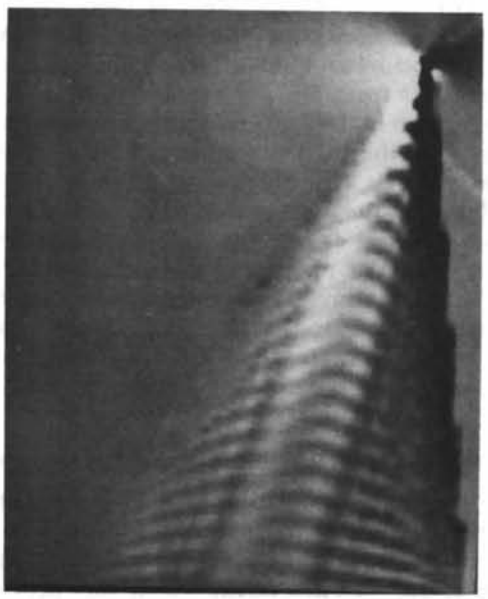

(*b*)

Fig. 5. Laue synchrotron topograph of a silicon crystal 800 μm thick. $\lambda = 0.71$ Å, 220 reflection. (*a*) Experiment: the studied dislocation is indicated by an arrow. (*b*) Simulation. Area 400 × 330 μm. Resolution 2 μm. One pixel in three is calculated along a line, one in two along a column, except near the direct image, where all pixels are calculated.

We have studied in detail the simulation of this critical part of the image. As previously explained, the best result is achieved by a combination of the Ψ and Φ methods and an automatic switching between them. However, it does not dramatically improve the present image, which is already good, since the maximum grey density is reached in this part of the image. Thus, our conclusion is that it is faster first to compute the image with the standard network. If the direct image seems to be wrong, it is necessary to compute this area again as explained above. For instance, we have simulated the image of the dislocation in quartz, which has been studied in the preceding paper (Carvalho & Epelboin, 1993). The dislocation lies parallel to the faces of the crystal and it appears as a dark straight line in the topograph. We had to use the second method to obtain a correct width for the image.

The computation of a traverse or synchrotron topograph remains a lengthy calculation. The image shown in Fig. 5 needs about 3 h CPU time on a superworkstation. This is much better than using the direct method, which needs tens of hours. The possibility offered by the reciprocal method to decouple the resolution from the integration steps allows crude simulations for a first study but we are far from the possibility of simulations in real time near a synchrotron Laue station. The simulation is now usable but for selected studies only.

Concluding remarks

It is now possible to simulate traverse and synchrotron topographs easily. The reciprocity theorem allows the resolution in the image to be decoupled from the size of the integration steps, so it is possible to choose its best value in all parts of an image. This not only speeds up the calculation but permits crude simulations with poor resolution in a reasonable time. It is up to the user to build up a strategy to save CPU time for a particular calculation; it will always be slow. Since our numerical algorithm is valid for extended defects, it is possible to simulate all kinds of defects as long as a valid deformation model is known. This means that it is now possible to extract quantitative information from a traverse or a synchrotron topograph as has long been possible from a section topograph. Since this last technique cannot be used in many cases, such as for thin crystals or for most experiments at a synchrotron station, the possibility of simulating the experiment will give the same help to the physicist as the previous simulations for section topographs.

CAMC acknowledges a doctorate scholarship from CNPq, Brazil.

References

AUTHIER, A., MALGRANGE, C. & TOURNARIE, M. (1968). *Acta Cryst.* A**24**, 126-136.
AUTHIER. A. & SIMON, D. (1968). *Acta Cryst.* A**24**, 517-526.
BALIBAR, F. (1969). *Acta Cryst.* A**25**, 650-658.
CARVALHO, C. A. M. & EPELBOIN, Y. (1990). *Acta Cryst.* A**46**, 449-459.
CARVALHO, C. A. M. & EPELBOIN, Y. (1993). *Acta Cryst.* A**49**, 460-467.
EPELBOIN, Y. (1977). *Acta Cryst.* A**33**, 758-767.
EPELBOIN, Y. & SOYER, A. (1985). *Acta Cryst.* A**41**, 67-72.
KATO, N. (1968). *Acta Cryst.* A**24**, 157-160.
LANDAU, L. & LIFCHITZ, E. (1960). *Electrodynamique des Milieux Continus.* Moscow: Mir.
PETRASHEN, P. V. (1976). *Sov. Phys. Solid State*, **18**, 2175-2176.
PETRASHEN, P. V., CHUKHOVSKII, F. N. & SHULPINA, I. L. (1980). *Acta Cryst.* A**36**, 287-295.
TAKAGI, S. (1969). *J. Phys. Soc. Jpn*, **26**, 1239-1253.
TAUPIN, D. (1967). *Acta Cryst.* **23**, 25-35.

Acta Cryst. (1993). A**49**, 473-480

Atomic Thermal Parameters and Thermodynamic Functions for Corundum (α-Al_2O_3) and Bromellite (BeO): a Lattice-Dynamical Estimate

BY TULLIO PILATI

CNR, Centro per lo Studio delle Relazioni tra Struttura e Reattività Chimica, Via Golgi 19, *I*-20133 *Milano, Italy*

FRANCESCO DEMARTIN

Istituto di Chimica Strutturistica Inorganica, Università degli Studi, Via Venezian 21, *I*-20133 *Milano, Italy*

AND CARLO MARIA GRAMACCIOLI

Dipartimento di Scienze della Terra, Sezione di Mineralogia, Università degli Studi, Via Botticelli 23, *I*-20133 *Milano, Italy*

(*Received* 7 *April* 1992; *accepted* 13 *October* 1992)

Abstract

A harmonic valence-force-field rigid-ion lattice-dynamical model fitted to Raman and IR spectral data and extended throughout the whole Brillouin zone has been used to calculate the atomic displacement parameters, entropy and molar heat capacity for corundum (α-Al_2O_3) and bromellite (BeO). The agreement with experimental data is good.

Introduction

In the last few years, the importance and physical significance of crystallographic atomic thermal parameters (or atomic displacement parameters, a.d.p.s) have been emphasized by chemists and physicists [see, for example, Pilati, Bianchi & Gramaccioli (1990*b*) and references therein]; at the same time, considerable interest in this subject has also been developed by mineralogists [see, for example, Downs, Gibbs & Boisen (1990) and references therein].

It is well known (Willis & Pryor, 1975) that theoretical estimates of a.d.p.s can be best obtained from lattice dynamics, following the procedure first described by Born & von Karman (1912, 1913) using a conveniently sampled set of values of the wave vector $\mathbf{q}$ in the Brillouin zone [corresponding to the reciprocal unit cell of the crystal; a recent discussion of such sampling is given by Pilati, Bianchi & Gramaccioli (1990*c*)]. For a particular value of $\mathbf{q}$ and for a harmonic model, the average energy $E_{\psi\mathbf{q}}$ of each normal mode ($\psi\mathbf{q}$) of frequency ν is

$$E_{\psi\mathbf{q}} = h\nu\{\tfrac{1}{2} + [\exp(h\nu/kT) - 1]^{-1}\}, \quad (1)$$

where h and k are the Planck and Boltzmann constants, respectively, and T is the absolute temperature. The limit as $\nu \to 0$ of the above expression is

$$\lim_{\nu\to 0} E_{\psi\mathbf{q}} = \lim_{\nu\to 0} [kT/\exp(h\nu/kT)], \quad (2)$$

which shows that the contribution to vibrational energy grows when the frequency is decreased. This happens because the lowest vibrational-energy levels are more populated than the highest levels, a phenomenon that is enhanced for low temperatures.

From these data and the mass-adjusted polarization vectors $\mathbf{e}_{p,\psi\mathbf{q}}$ of the atom p in the unit cell, which are part of the eigenvectors of the dynamical matrices $\mathbf{D}(\mathbf{q})$, the a.d.p.s $\mathbf{U}_p$ can be obtained as

$$\mathbf{U}_p = (Nm_p)^{-1} \sum_{\psi\mathbf{q}} E_{\psi\mathbf{q}} (2\pi\nu_{\psi\mathbf{q}})^{-2} \mathbf{e}_{p,\psi\mathbf{q}} \cdot \mathbf{e}^{*T}_{p,\psi\mathbf{q}}, \quad (3)$$

where N is the total number of unit cells in the crystal. The simulations are extended to all the vibrational

0108-7673/93/030473-08$06.00